

SAPO-37 microporous catalysts: revealing the structural transformations during template removal

Georgios N. Kalantzopoulos, Fredrik Lundvall, Anna Lind, Bjørnar Arstad, Dmitry Chernyshov, Helmer Fjellvåg & David S. Wragg

To cite this article: Georgios N. Kalantzopoulos, Fredrik Lundvall, Anna Lind, Bjørnar Arstad, Dmitry Chernyshov, Helmer Fjellvåg & David S. Wragg (2017) SAPO-37 microporous catalysts: revealing the structural transformations during template removal, *Catalysis, Structure & Reactivity*, 3:1-2, 79-88, DOI: [10.1080/2055074X.2016.1262569](https://doi.org/10.1080/2055074X.2016.1262569)

To link to this article: <https://doi.org/10.1080/2055074X.2016.1262569>



© 2017 The Author(s). Published by Informa UK Limited, trading as Taylor & Francis Group



[View supplementary material](#)



Published online: 22 Feb 2017.



[Submit your article to this journal](#)



Article views: 303



[View related articles](#)



[View Crossmark data](#)



Citing articles: 1 [View citing articles](#)

SAPO-37 microporous catalysts: revealing the structural transformations during template removal

Georgios N. Kalantzopoulos^a , Fredrik Lundvall^a , Anna Lind^b, Bjørnar Arstad^b, Dmitry Chernyshov^c, Helmer Fjellvåg^a and David S. Wragg^a

^aCentre for Materials Science and Nanotechnology (SMN), Department of Chemistry, University of Oslo, Oslo, Norway; ^bSINTEF Materials and Chemistry, Oslo, Norway; ^cSwiss-Norwegian Beamline, The European Synchrotron, Grenoble, France

ABSTRACT

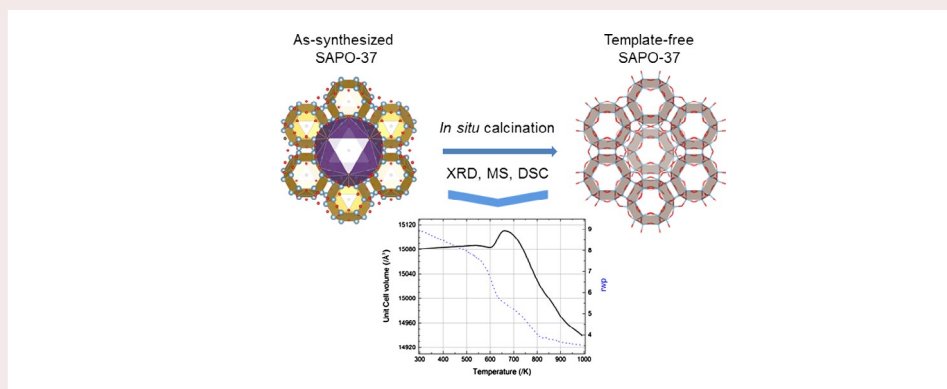
We have studied the structural behavior of SAPO-37 during calcination using simultaneous *in situ* powder X-ray diffraction (PXRD) and mass spectroscopy (MS) in addition to *ex situ* thermogravimetric analysis (TGA) and differential scanning calorimetry (DSC). A spike in the unit cell volume corresponding to template removal (tracked using the occupancy of the crystallographic sites in the SAPO-37 cages) is revealed from the XRD data and is strongly correlated with the DSC curve. The occupancy of the different template molecules in the faujasite (FAU) and sodalite (SOD) cages is strongly related to the two mass loss steps observed in the TGA data. The templates act as a physical stabilizing agent, not allowing any substantial unit cell response to temperature changes until they are removed. The FAU cages and SOD cages have different thermal response to the combustion of each template. The FAU cages are mainly responsible for the unit cell volume expansion observed after the template combustion. This expansion seems to be related with residual coke from template combustion. We could differentiate between the thermal response of oxygen and T-atoms. The T–O–T angle between two double 6-rings and a neighboring T–O–T linkage shared by SOD and FAU had different response to the thermal events. We were able to monitor the changes in the positions of oxygen and T-atoms during the removal of TPA⁺ and TMA⁺. Large changes to the framework structure at the point of template removal may have a significant effect on the long-term stability of the material in its activated form.

ARTICLE HISTORY

Received 30 September 2016
Accepted 15 November 2016

KEYWORDS

Faujasite; SAPO-37; *in situ* calcination; powder diffraction; rietveld refinement; zeolite; calorimetry; template removal




Introduction

Due to their acidic and shape-selective properties, zeolites have found widespread applications in catalytic, ion-exchange and separation processes in several industries [1]. Although the materials have been used at industrial scale since the 1980s [2], the exact changes template removal induces in the local structure and how they affect long-term stability after calcination still remains to be understood. Another class of materials similar to

zeolites is the Silicoaluminophosphates (SAPOs), a special class of porous materials similar to zeolites, where a framework of tetrahedrally oxygen-coordinated Al and P has been partially substituted by Si. The substitution of a pentavalent P-atom by a tetravalent Si-atom creates a charge deficiency which is balanced by a positively charged structure directing agent (SDA) during synthesis or a monovalent cation after the template removal during calcination [3]. When the cation is a proton,

CONTACT Georgios N. Kalantzopoulos  georgiok@smn.uio.no; David S. Wragg  david.wragg@smn.uio.no

 Supplemental data for this article can be accessed here. [<http://dx.doi.org/10.1080/2055074X.2016.1262569>]

© 2017 The Author(s). Published by Informa UK Limited, trading as Taylor & Francis Group.

This is an Open Access article distributed under the terms of the Creative Commons Attribution License (<http://creativecommons.org/licenses/by/4.0/>), which permits unrestricted use, distribution, and reproduction in any medium, provided the original work is properly cited.

a Brønsted acidic site is created [4]. The presence of Brønsted acidic sites on the walls of the SAPO framework is the origin of the catalytic activity used in the refining and petrochemical industries.

The material in this study, SAPO-37, has the faujasite (FAU) topology as found in zeolites X and Y. SAPO-37 crystallizes in the $Fd\bar{3}m$ space group and has a typical cubic unit cell dimension of $a = 24.345 \text{ \AA}$. FAU has a 3-D network of tetrahedral atoms (T-atoms, where T = Al, P or Si) which form sodalite cages linked by double 6-ring (d6r: meaning two rings of 6 T-atoms) units. These create a network of large cages (faujasite, FAU, cages) accessed by 12-ring windows. The 12-ring has a diameter of 11.2 \AA (distance across diametrically opposite oxygen atoms) and molecules with diameter of up to 7.3 \AA can diffuse along the channels [5]. These properties make zeolites X and Y and the related Ultrastable Y, excellent catalyst materials for crude oil processing [6,7]. They are used in processes such as the isomerization of *n*-decane [8], isobutane/2-butene alkylation [9], *o*-xylene isomerization [10] or as gas adsorbents [7]. Typical SAPO-37 synthesis routes involve the use of two structure directing agents, tetramethylammonium hydroxide (TMAOH) and tetrapropylammonium hydroxide (TPAOH). Depending on the synthesis route, SAPO-37 crystallizes from a semi-crystalline layered precursor containing large pores and sodalite cages or follows a “birth and spread” crystal growth mechanism [11]. Today it is largely accepted that TMAOH is responsible for the formation of the smaller sodalite cages where TPAOH is involved in the formation of the 12-ring FAU supercage [12]. Upon calcination of the as-synthesized material, one can monitor the removal of the two SDAs occurring in consecutive mass loss steps [12]. Although quite a lot is known about the SDA combustion temperature region and the gases evolved during the process, little is known about the local structural changes that the material undergoes upon the removal of the SDA. SAPO-37 is known to have poor stability below 345 K after calcination [13]. In contrast to the specific mixture of organic templates required to produce SAPO-37, aluminosilicate faujasites can be prepared with simple alkali/alkaline earth metal templates (as found in natural faujasite) which can be removed under mild conditions [14].

In a pioneering work from 1991, Briend et al. showed that TPA^+ in the SAPO-37 supercage decomposes in the 473–523 K temperature range *via* a series of β -eliminations releasing propene [15]. Furthermore, by applying *in situ* IR absorption spectroscopy the authors found that while calcining, TMA^+ begins its degradation at 523 K and continues its decomposition up to 823 K. During this period Brønsted acidic sites are formed during a Hofmann degradation step of the propylamine. As the combustion of both templates takes place, coke is formed. This is finally removed at 873 K. While performing *in situ* IR absorption spectroscopy during the

heating of as-synthesized SAPO-37 in N_2 , Corma et al. observed the formation of at least six types of hydroxyl groups at 573 K [16]. Terminal SiO-H and PO-H were detected and remained present up to the end of the heat treatment at 873 K. The other four hydroxyl species were bridging Si-OH-Al directed towards the supercage and to the sodalite cages, and two types of hydroxyls associated with the remaining organic templates. According to the above *in situ* IR study, condensation of the Si-OH and P-OH species could lead to formation of Si-O-P bonds with the latter being highly susceptible to hydrolysis upon exposure to water at near ambient temperature. After the material has cooled down to RT and been exposed to atmospheric air, H_2O molecules coordinated with -OH attached to the SAPO-37 structure and H_2O_5^+ species were detected. These species have been correlated with the low hydrothermal stability of the calcined material in atmospheric air.

SAPO-37 is synthesized using a well-defined mixture of TMA and TPA hydroxides as SDAs. Cross-polarization ^{13}C NMR experiments from earlier works showed a well-defined peak at 58.7 ppm ascribed to the TMA^+ ions in the sodalite cages [15]. Taking into consideration the pore opening of the 6-membered ring (2.8 \AA) and the effective diameter of TMA^+ (6.4 \AA) it appears that one TMA^+ ion can fit in the sodalite cage without being able to diffuse through it. TPA^+ is the template for the 12-membered ring and due to its size it can only fit in the supercage. Previous works have estimated that approximately 1.7 TPA^+ ions can fit in the supercage independent of the SAPO-37 Si content [17,18]. The SAPO-37 framework has a negative charge and requires compensating cations to balance the total charge [15,18]. In the as-synthesized SAPO-37, the charge compensating cations can be TMA^+ , TPA^+ or protons [15]. At this stage the material has neutral charge, and the SOD cages and FAU supercages are filled with organic templates. It is only after the calcination that the protonic sites are generated, providing the material with its acidic character [15]. The observations described above will be discussed in light of our own data.

Due to the need to study the environment around specific atoms, NMR has been the main probe for detecting local changes in SAPO materials. However, recent advances in synchrotron radiation powder XRD (SR-PXD) data acquisition have given a significant improvement in time resolution in this technique. This provides a new level of information on fundamental procedures such as template removal, revealing details previously impossible to see [19]. Here we present the findings of combined high time resolution SR-PXD/MS and DSC/TGA studies of template removal which reveal significant structural changes occurring around the point of template removal. These may be significant for our understanding of the long term stability of this material and other zeolite frameworks.

Experimental

SAPO-37 was synthesized according to literature procedures [20]. The molar ratios of the components in the final gel were 1.0 SiO₂: 1.0 Al₂O₃: 1.0 P₂O₅: 0.025 (TMA)₂O: 1.0 (TPA)₂O: 50 H₂O. Firstly, phosphoric acid (85% Merck) and deionized water were mixed at 293 K and alumina (Catapal, 72% Al₂O₃, SASOL) was then slowly added under vigorous stirring. The mixture was stirred for 8 h at 293 K in a temperature controlled bath. A second mixture was prepared by dissolving the tetramethylammonium hydroxide (TMAOH*5H₂O, 99% Aldrich) in the tetrapropylammonium hydroxide (TPAOH, 40% aqueous solution, Alfa). Silica (Aerosil 200, Degussa) was added to this solution under vigorous stirring, which was maintained for 1 h. Finally, the silicate solution was slowly added to the aluminate solution under vigorous stirring and the mixture was aged at 293 K in a temperature controlled bath under continuous stirring for 24 h. The aged gel was transferred into Teflon-lined autoclaves, heated up to 473 K and kept there for 13 h. After the reaction time, the autoclaves were quenched and the product was separated by centrifugation. The resulting powder was washed well with deionized water and dried at 353 K overnight.

Simultaneous thermogravimetric analysis (TGA) and differential scanning calorimetry (DSC) experiments were performed in a Netzsch STA 449 F1 instrument. The samples were measured in dry, Al₂O₃ crucibles and heated from 298 to 1273 K, with a heating rate of 5 K min⁻¹ under synthetic air (N₂/O₂ 80/20) (50 ml min⁻¹). The measurements were baseline corrected using the Proteus software package.

In situ SR-PXD measurements were performed at the Swiss–Norwegian beamline (station BM01A/BM01) at the European Synchrotron (ESRF) in Grenoble, France. A fresh as-synthesized SAPO-37 sample was placed in a 0.5 mm quartz capillary and mounted on a flow cell that

kept the capillary in controlled atmosphere. The sample was heated up to 1070 K at 2 K min⁻¹ using a hot air blower in flowing synthetic air. Temperature calibration was performed by measuring a sample of high purity Ag and Al₂O₃. The SR-PXD patterns (exposure time of 10 s) were collected using a Dectris Pilatus 2 M photon counting pixel area detector [21,22] and then integrated with the PyFAI program [23]. The wavelength, $\lambda = 0.71210$ Å was calibrated from individual runs with LaB₆. The patterns were analyzed by parametric Rietveld refinement [24] using TOPAS [25] to extract the unit cell parameters, framework atom positions, the isotropic thermal parameters (B-iso) and the template occupancy as a function of temperature. A single B-iso parameter was refined for all oxygen atoms. Difference Fourier maps were used to assign the positions of dummy carbon atoms in the voids and the occupancies of these were allowed to refine (with symmetry constraints) during subsequent cycles [26]. A Pfeiffer Omnistar GSD 301 T3 Quadrupole mass spectrometer was coupled at the exhaust line of the flow cell (sample to instrument distance <30 cm) for mass spectrometry data acquisition during the calcination process. The total acquisition and read out time of each of the acquired mass spectra was <0.8 s.

Results and discussion

In situ SR-PXD during calcination of SAPO-37 reveals a spike in unit cell volume at the temperature at which the oxidative thermal decomposition of template takes place (Figure 2, top). Earlier *in situ* studies of the same process in other zeolite systems had not captured this volume expansion in full detail due to the low time resolution in earlier SR-PXD data acquisition [19]. This new information allows us to observe the structural transformations the template removal induces on this material at a more detailed level.

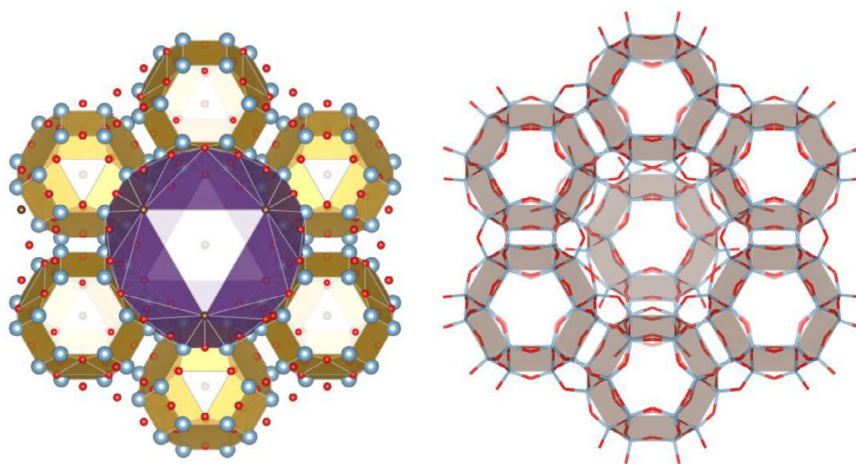


Figure 1. SAPO-37 viewed perpendicular to the (111) plane. Left: Colored polyhedra indicate the volume that each template can occupy (magenta for TPA⁺ in the FAU supercage and yellow for TMA⁺ in the SOD cages). Framework oxygens and T-atoms are indicated in red and blue, respectively. The brown spheres are carbon dummy atoms used to simulate the template occupancy in each cage. Right: SAPO-37 framework after template removal. The SOD cages are highlighted with translucent maroon polyhedra.

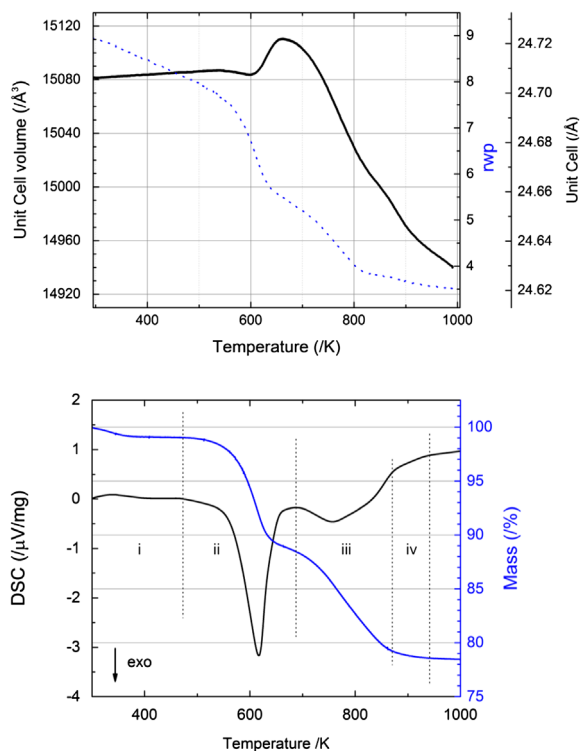


Figure 2. Top: Unit cell volume and Rwp variation extracted by parametric Rietveld refinement using TOPAS from *in situ* calcination at the Swiss-Norwegian beamline (BM01) at ESRF. The temperature range was 298–1000 K and the heating rate 2 K min^{-1} . The wavelength was 0.71210 \AA . Bottom: Combined TGA-DSC plots of as-synthesized SAPO-37 during heating. The temperature range was 298–1000 K and the heating rate 5 K min^{-1} .

The removal of physisorbed water from the external surface of the as-synthesized SAPO-37 takes place between RT and 375 K. It corresponds to a 2 wt% (zone i, Figure 2, bottom) mass loss without any impact on the unit cell dimensions. At 475 K the TPA^+ decomposition and removal from the supercages which constitute the main void volume of the material [12] begins and continues up to 690 K (zone ii, Figure 1, bottom). The event is accompanied by a major exothermic peak in the DSC and a prominent mass loss in the same temperature range in the TGA that accounts for 10.5 wt%. Between 690 and 945 K a second mass loss step of 9.9 wt% takes place (zones iii & iv, Figure 2, bottom). This step is associated with the removal of TMA^+ from the smaller sodalite cages [12]. In the DSC it is reflected by a weak, broad, exothermic peak taking place in the same temperature range. Past works have shown that the decomposition temperature of a given template may vary from framework to framework and strongly depends on the location in the framework, the geometry and the ion or cation local environment [27–29].

At 300 K the as-synthesised SAPO-37 has a unit cell with a volume of 15801 \AA^3 , corresponding to $a = 24.706 \text{ \AA}$ (Figure 2, top). As the temperature increases to 540 K, the unit cell volume increases to 15086 \AA^3 . At 600 K the

unit cell volume drops back to its initial value before we see a sharp increase to 15110 \AA^3 between 600 and 660 K. At this point the decomposition of TPA^+ has already progressed to some extent (initiated around 475 K) while the multi-step TMA^+ decomposition began at 523 K. The strong exothermic peak of the DSC (zone ii, Figure 1, bottom) has an onset temperature of 566 K and reaches its maximum at 617 K. In fact, this DSC peak is a convolution of two independent exothermic peaks, one related to the TPA^+ (main event at this region) and a second connected with the TMA^+ combustion that has already begun at that temperature region. Above 660 K two simultaneous and independent mechanisms take place: (i) the unit cell shrinking due to the physical removal of the decomposed templates (mainly TPA^+) and ii) the unit cell shrinking due to SAPO-37's negative thermal expansion. Calcined siliceous faujasite is known to have a strong isotropic negative thermal expansion coefficient attributed to transverse vibrations of the bridging oxygen atoms [30]. At this point it is interesting to note that practically no shrinkage is observed at 300–540 K where the framework is stabilized by the rigid, bulky organic templates.

As the combustion proceeds and the template is gradually removed from the faujasite pore network, the unit cell shrinks down to 14939 \AA^3 (minimum value for the investigated temperature range). The slightly faster heating rate used in the TGA/DSC experiments (5 vs. 2 K/min) means that the peaks of the thermal events are shifted a few kelvin higher than what we would expect to observe at 2 K/min . In the 300–1000 K region, there are only two broad thermal events. Therefore, conducting the TGA/DSC measurement at 2 K/min would not affect the quality of the results. In fact, both measurements were carried out in carefully calibrated experimental set-ups where special attention was paid to the simultaneous and homogeneous distribution of heat over the sample.

The SR-PXD data were further analyzed to obtain a higher degree of understanding on the changes the structure undergoes upon template removal. Firstly, the changes in thermal parameter B-iso of both oxygen and T-atoms are linked indicating a fairly consistent thermal behavior as the temperature increases (Figure 3, left). The thermal parameters remain at their set lower limits until 540 K for the oxygen atoms and 690 K for the T-atoms (minimum allowed value 1.0 \AA^3). At 540 K, the B-iso values for oxygen start increasing and at 690 K the same occurs for the B-iso values of the T-atoms as well. In the case of the oxygen atoms the B-iso values have two bumps in the 610–725 K and 800–945 K regions. The first coincides fairly well with the temperature of the main exothermic peak (617 K). The second overlaps with the second half of the second exothermic event observed in the DSC (Figure 2, bottom). At 550 K the B-iso value for oxygen has a non-linear behavior as the

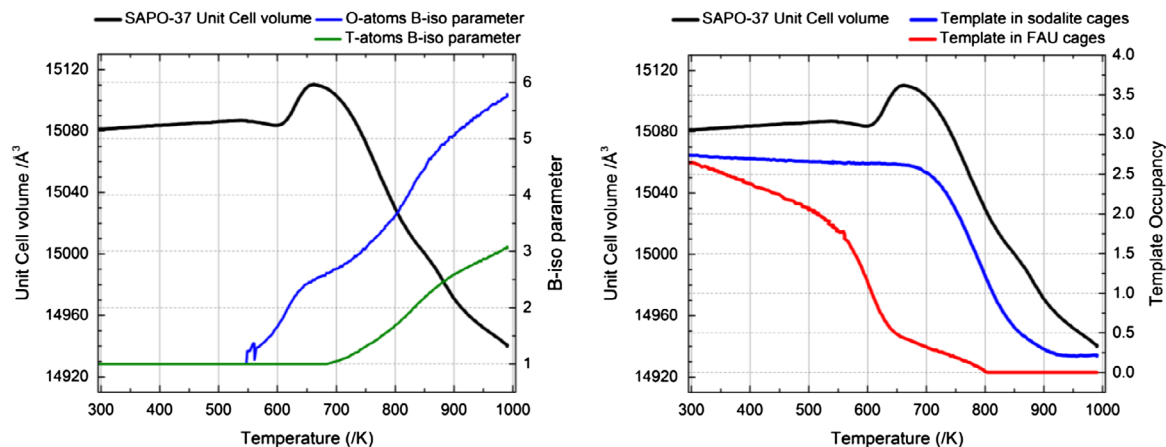


Figure 3. Parametric Rietveld refinement results illustrating the template removal evolution in the 298–1000 K temperature region. The values of SAPO-37 unit cell volume are presented in relation with the oxygen and T-atoms thermal parameter B-iso (left) and the occupancy of the dummy atom corresponding to each template, TMA⁺ in blue and TPA⁺ in red, respectively (right). Note that minimum limits of 1.0 Å³ were used for the B-iso values.

parameter value begins to increase. It coincides with the temperature at which the main exothermic event in the DSC begins, which indicates the beginning of TPA⁺ decomposition and combustion in the FAU supercage. Interestingly, there is a small non-linear behavior in the TPA⁺ template occupancy at the same temperature (Figure 3, right). This relatively violent movement of the oxygen atoms might indicate the breaking of the coordination between a terminal oxygen atom from the framework and the template as it starts its oxidative thermal decomposition. In this case, the movement may be connected with the formation of the acid site in the SAPO-37 framework.

The increase in the oxygen atoms thermal movement coincides with the temperature where TPA⁺ decomposition becomes significant (550 K). The B-iso value of the T-atoms does not change until immediately after the temperature where the spike in unit cell volume is observed in Figure 2 (660 K). Above this temperature it appears that the concerted actions of template removal and combustion significantly affect the vibrations of oxygen and T-atoms. The latter is expected to put strain on the local structure inside the unit cell and especially the supercage, which is the first region of the structure to lose its template. Our main motivation in these experiments was to monitor the structural changes the SAPO-37 unit cell undergoes during the template removal from the material cages. In the Rietveld refinement, the occupancy of the dummy carbon atoms was refined independently for each XRD pattern. As the temperature increases we can see a clear distinction between the occupancies of each template position (Figure 3, right). The template occupancy in the FAU cages begins to decrease above 400 K, however it is not until 520 K that the slope of the occupancy curve becomes significant. Up to 520 K the drop in FAU template occupancy does not have an observable effect on the mass loss (Figure 2, bottom), most likely because the

main part of TPA⁺ has not decomposed yet. The steepest gradient is found between 550 and 650 K, coinciding with the main exothermic event in the DSC (Figure 1, bottom). Above 650 K the TPA⁺ occupancy decreases at a lower rate until it reaches zero at 805 K. No significant drop in the occupancy values of TMA⁺ takes place up to 690 K. Between 690 and 940 K, the TMA⁺ occupancy decreases from 2.6 to 0.25 in a single step. Note that the precision of the refinements increases substantially above 620 K where most of TPA⁺ has been removed and the structure is closer to template-free SAPO-37 (rwp values Figure 2, top). Furthermore, the Rwp profile matches the TGA profile, which illustrates the template removal evolution as the temperature increases. The slightly higher Rwp values at low temperature are likely caused by the discrepancy between the simplified description of the TPA⁺ molecule by a single dummy carbon atom, and the actual shape and electronic density provided by the TPA⁺ molecule itself. As the occupancy goes down, this discrepancy will necessarily be significantly reduced.

The variation of selected T–O–T angles, T–T and O–O distances over the *in situ* calcination for the FAU and SOD cages are presented in Figure 4. As a typical T–O–T angle in the FAU cage we selected a T–O–T linkage in the d6r with the oxygen atom looking into the supercage (Figure 4(c)). Rather than monitoring the bond length of a given T–O pair we followed the variation of the FAU cage diameter using the distance of two diametrically opposite T–T and O–O pairs (Figure 4(d) and (e)). In the SOD cage, a T–O–T linkage shared between the FAU and SOD cages was selected (Figure 4(f)). The T–T distance of SOD cage T-atoms was monitored using T-atoms inside the cage (Figure 4(g)). Their relatively long distance from the FAU cage ensures the minimum possible interference with the thermal events occurring in the larger cage. Finally, a pair of neighboring, diametrically opposite oxygen atoms were selected to monitor the O–O distance in the SOD cage. As the

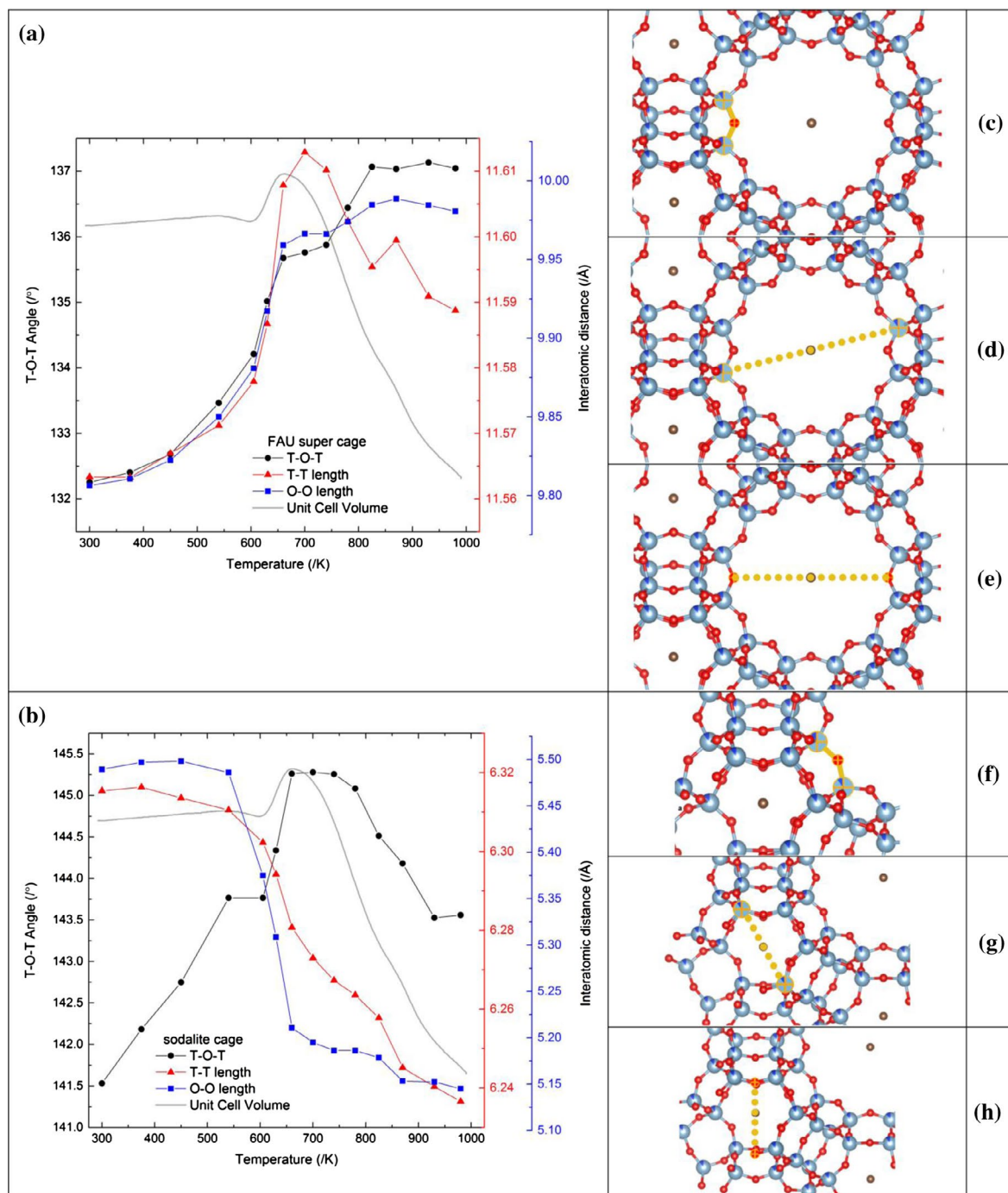


Figure 4. Variation of selected T–O–T angles, T–T and O–O distances for the FAU supercages (a) and the SOD cages (b). The selected T–O–T angle, T–T and O–O distances are illustrated in figures (c)–(e) for the FAU supercage and in figures (f)–(h) for the SOD cage, respectively. Blue spheres represent T-atoms; red, O-atoms and brown the dummy C-atoms used to model the template occupancy. In Figures (a) and (b) the unit cell volume variation is shown as a pale line for reference. The estimated standard deviations are below 0.015 Å for the distances and 0.4° for the angles.

temperature increases from 300 to 540 K there is an exponential increase in both T–O–T angle and T–T, O–O distances of the supercage. In the SOD cage the T–O–T angle increases in linear manner while no particular variation can be seen in its T–T and O–O distances. This suggests that the small volume increase observed in this temperature range should be attributed to thermal expansion of the organic templates, in particular TPA⁺ which occupies the biggest part of the available volume. Between 540 and 660 K the main exothermic

event takes place in the DSC. The response of the supercage to TPA⁺ combustion is a rapid expansion. In the SOD cage, the T–T and O–O distances have already started decreasing indicating that the decomposition of TMA⁺ has been initiated, as the earlier spectroscopic studies have shown [15]. Between 630 K and 740 K the O–O distance and T–O–T angle in the supercage remain essentially constant, whereas the T–T distance continues increasing, reaching its maximum close to 700 K. Similar behavior is observed in the neighboring T–O–T linkage,

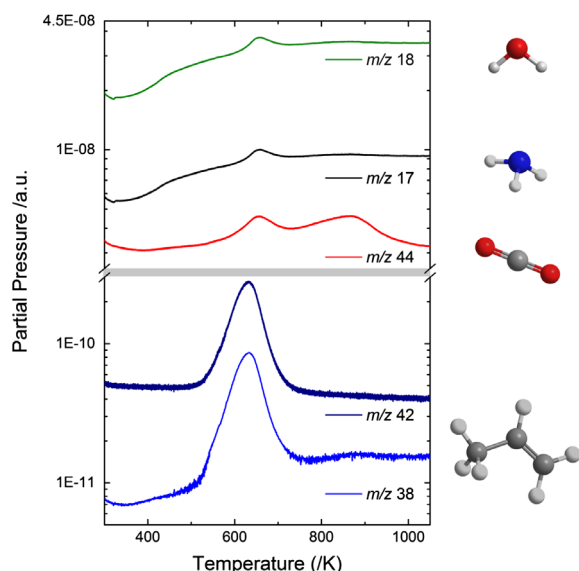


Figure 5. *In situ* mass spectroscopy data showing the evolution of masses 17, 18, 38, 42 & 44 during the calcination of as-synthesized SAPO-37. As shown in the scale, the signal of m/z 38 and 42 is two orders of magnitude smaller than the rest of the signals. The heating rate was 2 K min^{-1} .

shared by the FAU and SOD cages which reaches its maximum angle in the same temperature region. The T–T and O–O distance profile in the SOD cage follows the TMA^+ occupancy profile and both decrease rapidly above 600 K. This behavior indicates that the main spike in the unit cell volume is actually related to expansion of the supercage after the main DSC event. Above 800 K, the diameter of the supercage decreases as expected due to the material's negative thermal expansion coefficient, however, we do not observe any change in the T–O–T angle and O–O distance. At the same time, the T–O–T angle, T–T and O–O distances in the SOD cage continue decreasing as the TMA^+ occupancy drops. It is interesting to note that neighboring T–O–T linkages have a completely different response to the same thermal event. It seems that their behavior is dictated by the type of sub-framework units that are part of (FAU supercage vs. SOD cage vs. 6dr). Around 870 K a spike is observed in the T–T distance of both cages, correlating with the minor expansion observed in the unit cell volume at the same temperature (Figure 2, top).

Mass spectrometry data collected simultaneously during the *in situ* SR-PXD experiment are shown in Figure 5. Evolution of m/z 17 (mostly related with NH_3 species) and of m/z 18 (related with H_2O) begins as low as 380 K and exhibits a shoulder between 425 and 500 K. Between 620 and 690 K both signals show a peak that coincides with the spike in the unit cell at the same temperature range. m/z 44, that is strongly related with CO_2 begins its evolution at 520 K and has two peaks, one in the 600–700 K region and the second in the 700–850 K region. Each of these peaks is in very good agreement with the exothermic events observed in the DSC (Figure 2,

bottom) and is attributed to the combustion of each of the templates. It is interesting to note that both peaks coincide with the temperature region where the expansion of the supercage takes place, as indicated by the T–T distance (Figure 4(a)). Additionally, they fit with the two mass loss events observed in the TGA (Figure 2, bottom). Finally, between 500 and 730 K there is evolution of m/z 38 and m/z 42 which are related to the presence of propene in the detected ion species. Our mass spectra are thus in agreement with the results reported by Briend et al. [15]

The first mass loss step in the TGA curve occurs between 475 and 690 K. This should not be attributed purely to the oxidative thermal decomposition of TPA^+ , since this has initiated already at 523 K. There is a small expansion in the SAPO-37 unit cell up to 620 K, where more than half of the TPA^+ has been removed as Figure 3 (right) shows. Although most of TMA^+ has undergone decomposition and combustion, no unit cell changes can be seen until the FAU cage has been emptied of TPA^+ . At 620 K, where the TPA^+ dummy atom occupancy has dropped from 2.6 to 0.5, the framework responds to the thermal events and a clear lattice expansion begins to take place. That temperature coincides with the main exothermic event of the DSC plot. On the other hand, there is practically no change in the TMA^+ occupancy up to 690 K; the temperature where the second mass loss step begins in the TGA profile (Figure 2, bottom). This mass loss step corresponds to evolution of CO_2 , NH_3 , H_2O and propene-related species which account for 10.5 wt%. According to the spectroscopic studies of Briend et al. the oxidative decomposition of TMA^+ begins at 523 K and continues up to 823 K *via* a complex, multi-step reaction mechanism. According to our data, the decomposition of TMA^+ does not induce substantial changes in the unit cell up to 690 K where its occupancy clearly starts decreasing. This is also the temperature where the thermal parameter value of the T-atoms begins to increase. The increase in thermal movement of the oxygen atoms begins much earlier, however it is important to keep in mind that oxygen is coordinated with two T-atoms whereas each T-atom is surrounded by four oxygen atoms, leading to a much more rigid unit. The resistance of the tetrahedral unit to distortion has been illustrated in many studies of thermal expansion in zeolites [31,32]. Additionally, the formation of local defects (either temporary or permanent) on the framework as Corma et al. showed [16] could also be associated with the B-iso behavior of the oxygen atoms.

Between 690 and 945 K, TMA^+ is removed from the SOD cages. Its combustion is reflected by the DSC (Figure 2, bottom) and this affects the SAPO-37 unit cell volume which decreases from 15110 to 14939 \AA^3 . Between 825 and 925 K there is a shoulder on the unit cell volume plot of SAPO-37. This small decrease in the rate of unit cell shrinkage appears in the middle of the

second exothermic peak in the DSC signal. In a similar way, the main spike in the unit cell was also observed after the peak of the first exothermic event at 617 K. These two unit cell expansions cannot be in response to template combustion, because we would observe unit cell shrinkage due to the two exothermic events (negative thermal expansion). A possible explanation could be that the expansions are the material's response to gas released by template combustion that is trapped in the cages due to the continued presence of TMA⁺ in the sodalite cages. The gas can finally escape once most of the template has reacted and the SAPO-37 channels can be used by the evolved gaseous species. This can also explain the increase in the temperature where the main evolved gases (H₂O, NH₃ and CO₂) are detected; slightly after the main thermal events observed in the DSC have taken place. If this were the case, however, the effluent gases would be funneled through the supercage relatively quickly, even if half of it was still occupied by decomposing template molecules. A more reasonable explanation is the formation of coke during the combustion of each template. Coke will have little interaction with the framework, since the charge carrying nitrogen atoms left during the first thermal event (Figure 2, bottom and 5). In a similar manner, the minor local expansion of the SOD cages around 820 K could also be a response to coke accumulation as there is no second event in the NH₃ related *m/z* trace (Figure 5). During the *in situ* experiments, the powder took on a yellow tint between 473 and 523 K, its tone became darker as the temperature increased, then turned to black and finally white above 900 K. Coke formation leading to unit cell volume expansion has been observed for ZSM-5, SAPO-34 and SAPO-18 [29,33–36]. It is worth noticing that the unit cell shrinkage observed in this temperature region is attributed to two different, synergetic mechanisms: the template removal that physically empties the space in the sodalite cages and the material's intrinsic negative thermal expansion. In fact, it is only until the TPA⁺ has been substantially removed that we can observe the material shrinking due to negative thermal expansion and physical template removal. As long as the templates are present, they act as stabilizing agents, not allowing any unit cell response to temperature changes.

Compared to other frameworks, such as the hydrothermally stable SAPO-34, the calcination of SAPO-37 requires substantially higher temperatures for the combustion and complete removal of the templates (973 K instead of 823 K [37]). The higher temperatures required for the calcination induce structural rearrangements of the O and T-atoms which may make the material susceptible to rapid loss of crystallinity upon exposure to humid air at ambient temperature. It is also important to take into consideration the limitations of the PXRD method. The results obtained from PXRD (through the Rietveld refinement) give the time and space average positions as primary output. What we observe are

average changes in the local structure. If there are few and random faults in the structure, i.e. cleavage of some framework bonds, they would be challenging to identify. In their *in situ* IR work, Corma et al. showed that some permanent defects in the framework are formed [16]. As we can see in a short slide show (see Supplementary information) the local changes in the atomic positions around the point of template removal can be quite significant. Due to the fact that the template removal process takes place in hydrothermal conditions at particular elevated temperatures, the possibility that a temporary cleavage of some framework bonds cannot be excluded.

The selection of the suitable template or combination of templates, is a crucial parameter in zeolite synthesis that determines the nature of the final structure and its crystallinity [38]. According to the work of Davis and Lobo, templates can be classified into three different types [39]: (i) “true” templates, (ii) structure directing agents (SDAs) and (iii) space-filling species. Simulations using molecular dynamics to investigate the nature of the interaction between the formed zeolite framework and organic template show that the interaction is dominated by van der Waals bonding [40]. The term used by Stevens et al. to describe this interaction is “non-bonded” energy. Several experimental and theoretical works have demonstrated that for most zeolites, the better the template fills the void space the stronger the non-bonded energy will be [38]. Strong geometric match between template and framework is quite common in zeolites [41]. However ZSM-18, the one zeolite structure previously cited as the “known example of true templating”, has recently been prepared by a dual template method with a totally different and non-specific solvent-to-template ratio [42]. The different interactions which occur between the two templates and the cages they occupy, and the geometrical responses of the framework to the removal of the two templates may have a profound effect on the final calcined structure leading to the poor stability observed.

Conclusions

We have found evidence from several techniques that the two template types used to form the two different cages of SAPO-37 exhibit significantly different thermal behavior, and that their removal seems to be to some extent interdependent (the SOD cage cannot be cleared of template residues until the FAU cages are almost all empty). Furthermore the two cage types (as well as the linking d6r units) have different geometrical responses to the removal of their template molecules. Calcined SAPO-37 has limited stability at room temperature. This may be related in some way to the unusual progression of the template removal and the high temperatures required to drive out the residues from the smaller SOD cages. Aluminosilicate faujasite is highly stable, but is prepared with simple group I and II metal ion templates which can be removed under mild conditions. Compared to the

more stable SAPO-34 we also find that higher temperatures are required to remove the template from SAPO-37. It may be that the removal of template residues from the SOD cages of SAPO-37 at very high temperatures compared to other similar materials, combined with the major changes to the framework on template removal, leads in some way to its poor stability after calcination.

Acknowledgements

The research leading to these results was funded by the project “Catlife: Catalyst transformation and lifetime by *in situ* techniques and modelling”, P#233848” of the Research Council of Norway. We acknowledge the use of the Norwegian centre for X-ray diffraction and scattering (RECX). The authors thank the project team at the Swiss-Norwegian Beamline at the ESRF, France for their skillful assistance.

Disclosure statement

No potential conflict of interest was reported by the authors.

Funding

This work was supported by the Norges Forskningsråd [grant number 233848].

ORCID

Georgios N. Kalantzopoulos  <http://orcid.org/0000-0001-9213-9752>

Fredrik Lundvall  <http://orcid.org/0000-0002-0182-4437>

References

- [1] Vermeiren W, Gilson JP. Impact of zeolites on the petroleum and petrochemical industry. *Top Catal.* **2009**;52:1131–1161.
- [2] Chang CD. The New Zealand gas-to-gasoline plant: an engineering tour de force. *Catal Today.* **1992**;13:103–111.
- [3] Arstad B, Lind A, Cavka JH, et al. Structural changes in SAPO-34 due to hydrothermal treatment. An NMR, XRD, and DRIFTS study. *Microporous Mesoporous Mater.* **2016**;225:421–431.
- [4] Lok BM, Messina CA, Patton RL, et al. Silicoaluminophosphate molecular sieves: another new class of microporous crystalline inorganic solids. *J Am Chem Soc.* **1984**;106:6092–6093.
- [5] Baerlocher C, McCusker LB. Database of zeolite structures. Available from: <http://www.iza-structure.org/databases/>
- [6] Corma A, Diaz-Cabanas MJ, Martinez-Triguero J, et al. A large-cavity zeolite with wide pore windows and potential as an oil refining catalyst. *Nature.* **2002**;418:514–517.
- [7] Verboekend D, Nuttens N, Locus R, et al. Synthesis, characterisation, and catalytic evaluation of hierarchical faujasite zeolites: milestones, challenges, and future directions. *Chem Soc Rev.* **2016**;45:3331–3352.
- [8] Martens JA, Grobet PJ, Jacobs PA. Catalytic activity and Si, Al, P ordering in microporous silicoaluminophosphates of the SAPO-5, SAPO-11, and SAPO-37 type. *J Catal.* **1990**;126:299–305.
- [9] Mostad HB, Stocker M, Karlsson A, et al. Comparison of the iso-structural H-SAPO-37 and H-faujasite as catalysts for the isobutane/2-butene alkylation. *Appl Catal A.* **1996**;144:305–317.
- [10] Ojo AF, Dwyer J, Dewing J, et al. Synthesis and properties of SAPO-37. *J Chem Soc, Faraday Trans.* **1991**;87:2679–2684.
- [11] Zhang L, Chen D, Nie H-Y, et al. A study of the formation of microporous material SAPO-37. *Microporous Mesoporous Mater.* **2013**;175:147–156.
- [12] Yadav R, Ahmed M, Singh AK, et al. In-situ preparation of functionalized molecular sieve material and a methodology to remove template. *Sci Rep.* **2016**;6:22813.
- [13] Briend M, Shikholeslami A, Peltre M-J, et al. Thermal and hydrothermal stability of SAPO-5 and SAPO-37 molecular sieves. *J Chem Soc, Dalton Trans.* **1989**;1361–1362.
- [14] Klotz MR. Synthesis of crystalline aluminosilicate molecular sieves. Google Patents. **1983**.
- [15] Briend M, Lamy A, Peltre M-J, et al. Thermal stability of tetrapropylammonium (TPA) and tetramethylammonium (TMA) cations occluded in SAPO-37 molecular sieves. *Zeolites.* **1993**;13:201–211.
- [16] Corma A, Fornés V, Franco MJ, et al. Hydrothermal stability and cracking behavior of silicoaluminophosphate molecular sieve-37 with different silicon contents. Washington (DC): American Chemical Society; **1991**. Fluid Catalytic Cracking II. Vol. 452; p. 79–95.
- [17] de Saldarriaga Sierra L, Saldarriaga C, Davis ME. Investigations into the nature of a silicoaluminophosphate with the faujasite structure. *J Am Chem Soc.* **1987**;109:2686–2691.
- [18] Peltre MJ, Briend M, Lamy A, et al. Interaction of SAPO-37 molecular sieves with basic molecules: enhancement of stability. *J Chem Soc, Faraday Trans.* **1990**;86:3823–3826.
- [19] Milanese M, Artioli G, Gualtieri AF, et al. Template burning inside TS-1 and Fe-MFI molecular sieves: an *in Situ* XRPD study. *J Am Chem Soc.* **2003**;125:14549–14558.
- [20] Franco MJ, Pérez-Pariente J, Misud A, et al. Crystallization kinetics of SAPO-37. *Zeolites.* **1992**;12:386–394.
- [21] ESRF Swiss-Norwegian Beamline (BM01A). Available from: <http://www.esrf.eu/UsersAndScience/Experiments/CRG/BM01/bm01-a/image.htm>.
- [22] Dyadkin V, Pattison P, Dmitriev V, et al. A new multipurpose diffractometer PILATUS@SNBL. *J Synchrotron Radiat.* **2016**;23:825–829.
- [23] PyFAI, a python tool for fast azimuthal integration. Available from: <http://www.esrf.eu/UsersAndScience/Publications/Highlights/2012/et/et3/>
- [24] Stinton GW, Evans JSO. Parametric rietveld refinement. *J Appl Crystallogr.* **2007**;40:87–95.
- [25] TOPAS 5.0, Bruker AXS. **2012**. Available from: <http://www.topas-academic.net/>
- [26] Wragg DS, Akporiaye D, Fjellvåg H. Direct observation of catalyst behaviour under real working conditions with X-ray diffraction: comparing SAPO-18 and SAPO-34 methanol to olefin catalysts. *J Catal.* **2011**;279:397–402.
- [27] Bilger S, Soulard M, Kessler H, et al. Identification of the volatile products resulting from the thermal decomposition of tetra-, tri-, di-, and mono-n-propylammonium cations occluded in MFI-type zeolites. *Zeolites.* **1991**;11:784–791.

- [28] Soulard M, Bilger S, Kessler H, et al. Thermoanalytical characterization of MFI-type zeolites prepared either in the presence of OH- or of F-ions. *Zeolites*. **1987**;7:463–470.
- [29] Soulard M, Bilger S, Kessler H, et al. Characterization of the products remaining in the solid after partial thermal decomposition of Pr4NF-, Pr3NHF-, and Pr4NOH-MFI precursors. *Zeolites*. **1991**;11:107–115.
- [30] Attfield P. Strong negative thermal expansion in siliceous faujasite. *Chem Commun*. **1998**;601–602.
- [31] Wragg DS, Morris RE, Burton AW. Pure silica zeolite-type frameworks: a structural analysis. *Chem Mat*. **2008**;20:1561–1570.
- [32] Fütterer K, Depmeier W, Altorfer F, et al. Compression mechanism in trioxane silica sodalite, [Si12O24] ··· 2 C3H6O3. *Zeitschrift für Kristallographie – Cryst Mater*. **1994**;209:517–523.
- [33] Zokaie M, Wragg DS, Grønvold A, et al. Unit cell expansion upon coke formation in a SAPO-34 catalyst: a combined experimental and computational study. *Microporous Mesoporous Mater*. **2013**;165:1–5.
- [34] Wragg DS, Johnsen RE, Balasundaram M, et al. SAPO-34 methanol-to-olefin catalysts under working conditions: a combined *in situ* powder X-ray diffraction, mass spectrometry and Raman study. *J Catal*. **2009**;268:290–296.
- [35] Wragg DS, O'Brien MG, Bleken FL, et al. Watching the methanol-to-olefin process with time- and space-resolved high-energy operando X-ray diffraction. *Angew Chem Int Ed*. **2012**;51:7956–7959.
- [36] Wragg DS, Bleken FL, O'Brien MG, et al. The fast Z-scan method for studying working catalytic reactors with high energy X-ray diffraction: ZSM-5 in the methanol to gasoline process. *Phys Chem Chem Phys*. **2013**;15:8662–8671.
- [37] Wragg DS, Grønvold A, Voronov A, et al. Combined XRD and Raman studies of coke types found in SAPO-34 after methanol and propene conversion. *Microporous Mesoporous Mater*. **2013**;173:166–174.
- [38] Cundy CS, Cox PA. The hydrothermal synthesis of zeolites: precursors, intermediates and reaction mechanism. *Microporous Mesoporous Mater*. **2005**;82:1–78.
- [39] Davis ME, Lobo RF. Zeolite and molecular sieve synthesis. *Chem Mat*. **1992**;4:756–768.
- [40] Stevens AP, Gorman AM, Freeman CM, et al. Prediction of template location via a combined Monte Carlo-simulated annealing approach. *J Chem Soc, Faraday Trans*. **1996**;92:2065–2073.
- [41] Bu X, Feng P, Stucky GD. Host-guest symmetry and charge matching in two germanates with intersecting three-dimensional channels. *Chem Mat*. **2000**;12:1505–1507.
- [42] Burton AW, Vroman HB. Zeolite ZSM-18, its synthesis and its use. Google Patents. **2015**.